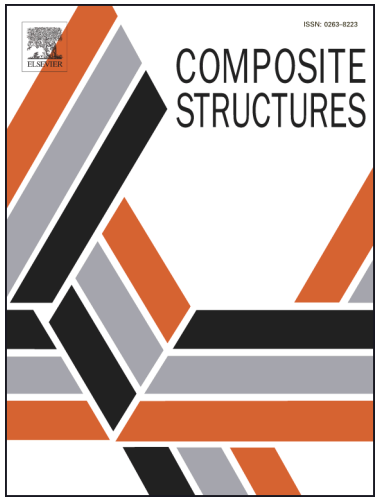

Phase-field thermal buckling analysis for cracked functionally graded composite plates considering neutral surface

Thom Van Do, Duc Hong Doan, Nguyen Dinh Duc, Tinh Quoc Bui

PII: S0263-8223(17)32383-8
DOI: https://doi.org/10.1016/j.compstruct.2017.09.059
Reference: COST 8922

To appear in: *Composite Structures*

Received Date: 28 July 2017
Revised Date: 16 September 2017
Accepted Date: 20 September 2017

Please cite this article as: Van Do, T., Doan, D.H., Duc, N.D., Bui, T.Q., Phase-field thermal buckling analysis for cracked functionally graded composite plates considering neutral surface, *Composite Structures* (2017), doi: https://doi.org/10.1016/j.compstruct.2017.09.059

Phase-field thermal buckling analysis for cracked functionally graded composite plates considering neutral surface

Thom Van Do[a], Duc Hong Doan[b,*], Nguyen Dinh Duc[b,c], Tinh Quoc Bui[d,e,*]

[a]*Department of Mechanics, Le Quy Don Technical University, Hanoi, Vietnam*
[b]*Advanced Materials and Structures Lab, University of Engineering and Technology, Vietnam National University, Hanoi, Vietnam*
[c]*Vietnam-Japan University, Vietnam National University, Hanoi, Vietnam*
[d]*Institute for Research and Development, Duy Tan University, Da Nang City, Vietnam*
[e]*Department of Civil and Environmental Engineering, Tokyo Institute of Technology, 2-12-1-W8-22, Ookayama, Meguro-ku, Tokyo 152-8552, Japan*

*Corresponding authors
Emails: doan.d.aa.eng@gmail.com (D. H. Doan); buiquoctinh@duytan.edu.vn; bui.t.aa@m.titech.ac.jp (T.Q. Bui)

Abstract

In this paper, the variational phase field model is adopted to analyze thermal buckling behavior of cracked functionally graded material (FGM) plates. Unlike existing works, the difference between neutral surface and mid-surface of FGM plates is taken into account in the present study. The kinematics of plate is based on first order shear deformation theory, while the crack is simulated by variational phase-field theory. The critical buckling temperature rises of cracked FGM plate is calculated, and the obtained results are then compared with those derived from extended isogeometric analysis by the authors and other numerical methods. We analyze the thermal buckling of cracked FGM plates for both cases: (a) the mid-surface coincides neutral surface, and (b) they are different between each other, and then showing their influence. We also investigate the effects of boundary condition and material properties on thermal buckling of cracked FGM plate. Through these results, it reveals the necessity to consider the difference between neutral surface and mid-surface in thermal buckling analysis.

Keywords: phase field model, thermal buckling, crack, Mindlin, neutral surface, functionally graded material

1. Introduction

Composite functionally graded material (FGM) has been increasingly used in a wide range of engineering applications. It is often made of the mixture of metal and ceramic, so that

the material properties vary smoothly from bottom to top surface. FGM often operates in high temperature environment, see for instance [1-5] and references therein. One common application of the FGM is some components of space vehicles and high-speed aircraft, which are usually subjected to elevated temperature. In such severe conditions, the high temperature often induces thermal stresses and once they are large enough, undesirable thermal buckling may occur, which results in the reduction of load carrying capacity, the performance of the structure, or even the failure of structures and devices.

In the past decades, the mechanical behavior of FGM plates has been accomplished by many researchers. The authors applied the extended isogeometric analysis (XIGA) to explore the thermal buckling of FG plates with internal defects [1]. They also analyzed the high temperature mechanical behavior of FGM plates using FEM and a new third-order shear deformation plate theory (TSDT) [2]. Javaheri and Eslami [6] studied thermal buckling of FG plates based on the analytical solution, and they later applied their analytical solution to study the mechanical and thermal buckling of thick FG plate based on a TSDT. Woo and Meguid [8] studied thermo-mechanical post-buckling of FG shells and plates. Najafideh and Heydari [9] used the TSDT to investigate thermal buckling of FG circular plate. Khalfi et al. [10] presented thermal buckling of solar FG plates resting on elastic foundation based on a refined shear deformation theory. Malekzadeh [11] applied a 3D elasticity theory to analyze thermal buckling of FG straight-sided quadrilateral plates. Shariat and Eslami [12] investigated the effects of geometrical imperfections on thermal buckling of FG plates. Jaberzadeh et al [13] explored the thermal buckling of FG skew and trapezoidal plates using a meshfree Galerkin method. Based on first order shear deformation theory (FSDT) and the element-free kp-Ritz method, Zhao et al. [14] investigated the mechanical and thermal buckling of FG plates.

It is important to note that the neutral surface and the mid-surface are identical in homogeneous plates, however, they are different is composite FGM plates. This discrepancy is important and its effects on mechanical and buckling behaviors of FGM plates are necessary to be explored. Some authors have been analyzing this problem. Zang [15] studied the effect of the neutral surface on thermal buckling of FGM plates using a high order shear deformation theory. Zhang and Zhou [16] presented a theoretical analysis of thin FG plates based on physic neutral surface. Yaghoobi and Fereidoon [17] investigated the influence of neutral surface position on the deflection of FGM beams. Young-Hoon Lee et al. [4] studied thermal buckling

of FGM plates based on the FSDT and neutral surface.

Some common methods such as FEM, XFEM [21-24], IGA, and phase field method have been developed for studying the fracture problems in engineering material and structures. The objective of this paper is to adopt the recently developed phase-field method [18-20] to study the thermal buckling of cracked FGM plates based on the FSDT theory, considering the neutral surface. The phase field model has proved to be a robust numerical technique for fracture modeling, which is very effective as no ad hoc criteria are required to track the evolution crack. Instead, the phase field model is based on the energy minimization concept, in which a phase field parameter is introduced to let crack grows along a path of least energy. In addition, one more advantages of the phase field method is that it is able to simulate complex fracture (e.g., multiple cracks) in 2D and 3D accurately. More detail of the phase field models and their advantageous features can be found in [18-20] and references therein. In this work, the neutral surface is considered to be not the same as the mid-plane of the plate because the material is not symmetric in the thickness direction. We analyze the thermal buckling of cracked FGM plates for both cases: (a) the mid-surface coincides neutral surface, and (b) they are different between each other. Numerical results of thermal buckling of cracked FGM plates are compared for two cases with and without the difference between neutral surface and mid-plane, and then conclude that in what condition one can neglect the difference or not. The effects of boundary conditions and some numerical aspects on the thermal buckling of cracked FGM plates are also analyzed. All this information may be helpful in the design of FGM for engineering applications.

The rest of the paper is organized as follows. We briefly present Reissner-Mindlin plate theory for FGM plates in Section 2. In Section 3, formulation of phase field model for cracked plates is presented. Numerical examples are presented and discussed in Section 4. Some major conclusions drawn from the study are given in Section 5.

2. Reissner-Mindlin plate theory of FGM plates

Material properties of FG plates are usually assumed vary in the volume fractions in the plate thickness. Let us consider a ceramic-metal FG plate with thickness h as depicted in Fig. 1, assuming that its bottom and top faces are to be fully metallic and ceramic, respectively [1-5]. In

this paper, the common simple power-law for describing the volume fraction of the ceramic (V_c) and the metal (V_m) is taken [1-3]:

$$V_c = \left(\frac{z}{h} + \frac{1}{2}\right)^n ;\ V_m = 1 - V_c \text{ with } n \geq 0 \tag{1}$$

where z is the thickness coordinate variable with $-h/2 \leq z \leq h/2$, and subscripts c and m represent the ceramic and metal constituents, respectively, n is the non-negative volume fraction gradient index.

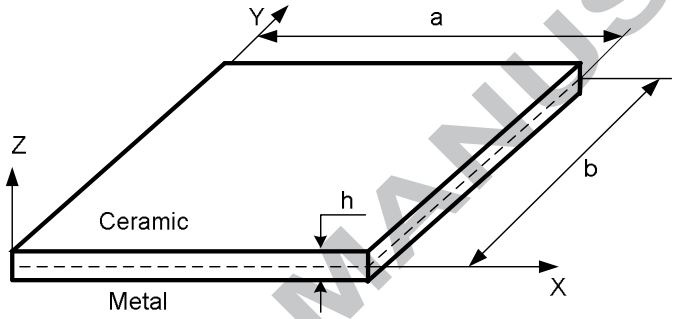

Fig. 1 Geometrical notation of a rectangular FGM plate.

According to the Reissner-Mindlin formulation, the displacement field is expressed as

$$\begin{aligned} u(x,y,z) &= u_0(x,y) + (z - h_0)\phi_x(x,y) \\ v(x,y,z) &= v_0(x,y) + (z - h_0)\phi_y(x,y) \\ w(x,y,z) &= w_0(x,y) \end{aligned} \tag{2}$$

where u, v, w are the displacements components in the x, y, z axes, respectively. ϕ_x, ϕ_y are the transverse normal rotations in the xz- and yz- planes; u_0, v_0, w_0 are displacement of neutral surface; h_0 is the distance between mid-surface and neutral surface, which is then calculated as follows [4]:

$$h_0 = \int_{-0.5h}^{0.5h} E(z).z dz \Big/ \int_{-0.5h}^{0.5h} E(z) dz \tag{3}$$

From Eq. (3), it reveals that h_0 only depends on the Young modulus of metal and ceramic, if the value of E_c/E_m ratio increases, then the value of h_0 also increases.

The strains in terms of mid-plan deformation can be expressed as follows:

$$\boldsymbol{\varepsilon} = \begin{Bmatrix} \boldsymbol{\varepsilon}_p \\ \mathbf{0} \end{Bmatrix} + \begin{Bmatrix} (z-h_0)\boldsymbol{\varepsilon}_b \\ \boldsymbol{\gamma}_s \end{Bmatrix} \tag{4}$$

where the vector $\boldsymbol{\varepsilon}_p$, $\boldsymbol{\varepsilon}_b$, $\boldsymbol{\gamma}_s$, $\boldsymbol{\varepsilon}_{th}$ contain a membrane, bending, transverse and thermal strain of the plate, respectively.

$$\boldsymbol{\varepsilon}_p = \begin{Bmatrix} u_{0,x} \\ v_{0,y} \\ u_{0,y} + v_{0,x} \end{Bmatrix};\ \boldsymbol{\varepsilon}_b = \begin{Bmatrix} \phi_{x,x} \\ \phi_{y,y} \\ \phi_{x,y} + \phi_{y,x} \end{Bmatrix};\ \boldsymbol{\gamma}_s = \begin{Bmatrix} \phi_x + w_{0,x} \\ \phi_y + w_{0,y} \end{Bmatrix} \tag{5}$$

The potential energy for plate subjected to in plane pre-buckling stress can be expressed as

$$\begin{aligned} U(\mathbf{u}) = {} & \frac{1}{2}\int_\Omega \left\{ \boldsymbol{\varepsilon}_p^T \mathbf{A} \boldsymbol{\varepsilon}_p + \boldsymbol{\varepsilon}_p^T \mathbf{B} \boldsymbol{\varepsilon}_b + \boldsymbol{\varepsilon}_b^T \mathbf{B} \boldsymbol{\varepsilon}_p + \boldsymbol{\varepsilon}_b^T \mathbf{D} \boldsymbol{\varepsilon}_b + \boldsymbol{\gamma}_s^T \mathbf{D}_s \boldsymbol{\gamma}_s \right\} d\Omega + \\ & + \frac{1}{2}\int_\Omega \begin{bmatrix} w_{,x} & w_{,y} \end{bmatrix} \hat{\boldsymbol{\sigma}}^0 \begin{bmatrix} w_{,x} & w_{,y} \end{bmatrix}^T h d\Omega + \frac{1}{2}\int_\Omega \begin{bmatrix} \phi_{x,x} & \phi_{x,y} \end{bmatrix} \hat{\boldsymbol{\sigma}}^0 \begin{bmatrix} \phi_{x,x} & \phi_{x,y} \end{bmatrix}^T \frac{h^3}{12} d\Omega + \\ & + \frac{1}{2}\int_\Omega \begin{bmatrix} \phi_{y,x} & \phi_{y,y} \end{bmatrix} \hat{\boldsymbol{\sigma}}^0 \begin{bmatrix} \phi_{y,x} & \phi_{y,y} \end{bmatrix}^T \frac{h^3}{12} d\Omega \\ = {} & \int_\Omega \Psi(\mathbf{u}) d\Omega \end{aligned} \tag{6}$$

wher $\mathbf{u}$ is the displacement vector; The matrices $\mathbf{A}$, $\mathbf{B}$, $\mathbf{D}$ and $\mathbf{D}_s$ are the extensional, bending-extensional coupling and bending stiffness coefficients and are explicitly given by

$$\{\mathbf{A},\ \mathbf{B},\ \mathbf{D}\} = \int_{-0.5h}^{0.5h} \frac{E(z)}{(1-\nu^2(z))} \begin{bmatrix} 1 & \nu(z) & 0 \\ \nu(z) & 1 & 0 \\ 0 & 0 & \dfrac{(1-\nu(z))}{2} \end{bmatrix} \{1, (z-h_0), (z-h_0)^2\} dz; \tag{7a}$$

$$\mathbf{D}_s = \int_{-0.5h}^{0.5h} \frac{kE(z)}{2(1+\nu(z))} \begin{bmatrix} 1 & 0 \\ 0 & 1 \end{bmatrix} dz;\ \hat{\boldsymbol{\sigma}}^0 = \begin{bmatrix} \sigma_x^0 & 0 \\ 0 & \sigma_y^0 \end{bmatrix};\ \sigma_x^0 = \sigma_y^0 = \frac{N^0}{h};\ N^0 = \int_{-0.5h}^{0.5h} \frac{E(z)}{1-\nu(z)} \alpha(z) \Delta T . dz \tag{7b}$$

where h is the thickness of plate, E is the elastic modulus, and k is the transverse shear correction factor. In this work, k=5/6 is used.

3. Formulation of phase-field model for cracked Reissner-Mindlin plates

In terms of phase-field theory of fracture [18-20], s is defined as a phase-field parameter, getting the value from 0 to 1. When s is equal to 0, it means that material phase is completely damaged, and it is intact when s is equal to 1. If s gets value between 0 and 1, then the material is in softening or "diffusive". This phase is understood as a progress of micro-crack in material and material stiffness decreases. Consequently, the crack in terms of phase field theory is modeled by a narrow zone. Phase-field variable is taken in strain energy formula of plate by s^2 function in Eq. (6), it means that the strain energy in cracked area are decreased to 0.

The potential energy for plates subjected to in plane pre-buckling stress because of temperature can be written as

$$\begin{aligned} U(\mathbf{u},s) &= \left\{ \begin{array}{l} \frac{1}{2}\int_\Omega s^2 \left\{ (\boldsymbol{\varepsilon}_p^T - \boldsymbol{\varepsilon}_{th}^T)\mathbf{A}(\boldsymbol{\varepsilon}_p - \boldsymbol{\varepsilon}_{th}) + \boldsymbol{\varepsilon}_p^T \mathbf{B}\boldsymbol{\varepsilon}_b + \boldsymbol{\varepsilon}_b^T \mathbf{B}\boldsymbol{\varepsilon}_p + \boldsymbol{\varepsilon}_b^T \mathbf{D}\boldsymbol{\varepsilon}_b + \boldsymbol{\gamma}_s^T \mathbf{D}_s \boldsymbol{\gamma}_s \right\} d\Omega + \\ \quad + \frac{1}{2}\int_\Omega s^2 \begin{bmatrix} w_{,x} & w_{,y} \end{bmatrix} \hat{\boldsymbol{\sigma}}^0 \begin{bmatrix} w_{,x} & w_{,y} \end{bmatrix}^T h d\Omega + \frac{1}{2}\int_\Omega s^2 \begin{bmatrix} \phi_{x,x} & \phi_{x,y} \end{bmatrix} \hat{\boldsymbol{\sigma}}^0 \begin{bmatrix} \phi_{x,x} & \phi_{x,y} \end{bmatrix}^T \frac{t^3}{12} d\Omega + \\ \quad + \frac{1}{2}\int_\Omega s^2 \begin{bmatrix} \phi_{y,x} & \phi_{y,y} \end{bmatrix} \hat{\boldsymbol{\sigma}}^0 \begin{bmatrix} \phi_{y,x} & \phi_{y,y} \end{bmatrix}^T \frac{t^3}{12} d\Omega + \int_\Omega G_C h \left[\frac{(1-s)^2}{4l} + l|\nabla s|^2 \right] d\Omega \end{array} \right\} \\ &= \left\{ \int_\Omega s^2 \Psi(\mathbf{u}) d\Omega + \int_\Omega G_C h \left[\frac{(1-s)^2}{4l} + l|\nabla s|^2 \right] d\Omega \right\} \end{aligned} \tag{8}$$

where G_c is the critical energy release rate or surface energy in terms of Griffith's theory and l is a positive regularization constant to regulate the size of the fracture zone.

The first variation of the functional $U(\mathbf{u},s)$ is given by

$$\begin{cases} \delta U(\mathbf{u},s,\delta\mathbf{u}) = 0 \\ \delta U(\mathbf{u},s,\delta s) = 0 \end{cases} \tag{9}$$

and then the formulations for pre-buckling analyses of cracked FGM plate is described as

$$\begin{cases} \left(\sum \mathbf{K}^e + \lambda_{cr} \sum \mathbf{K}_G^e \right) \mathbf{u} = 0 \\ \int_\Omega 2s\Psi(\mathbf{u}) \delta s d\Omega + \int_\Omega 2G_C h \left[-\frac{(1-s)}{4l} + l\nabla s \nabla(\delta s) \right] d\Omega = 0 \end{cases} \tag{10}$$

where:

$$\boldsymbol{K}^{\mathrm{e}} = \int_{\Omega_{\mathrm{e}}} \mathrm{s}^2 \boldsymbol{\varepsilon}_{\mathrm{p}}^{\mathrm{T}} \mathbf{A} \boldsymbol{\varepsilon}_{\mathrm{p}} \mathrm{d}\Omega + \int_{\Omega_{\mathrm{e}}} \mathrm{s}^2 \boldsymbol{\varepsilon}_{\mathrm{b}}^{\mathrm{T}} \boldsymbol{B} \boldsymbol{\varepsilon}_{\mathrm{p}} \mathrm{d}\Omega + \int_{\Omega_{\mathrm{e}}} \mathrm{s}^2 \boldsymbol{\varepsilon}_{\mathrm{p}}^{\mathrm{T}} \boldsymbol{B} \boldsymbol{\varepsilon}_{\mathrm{b}} \mathrm{d}\Omega + \int_{\Omega_{\mathrm{e}}} \mathrm{s}^2 \boldsymbol{\varepsilon}_{\mathrm{b}}^{\mathrm{T}} \boldsymbol{D} \boldsymbol{\varepsilon}_{\mathrm{b}} \mathrm{d}\Omega + \int_{\Omega_{\mathrm{e}}} \mathrm{s}^2 \boldsymbol{\varepsilon}_{\mathrm{s}}^{\mathrm{T}} \boldsymbol{D}_{\mathrm{s}} \boldsymbol{\varepsilon}_{\mathrm{b}} \mathrm{d}\Omega \tag{11}$$

$$\boldsymbol{K}_{\mathrm{G}}^{\mathrm{e}} = \int_{\Omega} \mathrm{s}^2 \begin{bmatrix} \mathrm{w}_{,\mathrm{x}} & \mathrm{w}_{,\mathrm{y}} \end{bmatrix} \hat{\boldsymbol{\sigma}}^0 \begin{bmatrix} \mathrm{w}_{,\mathrm{x}} & \mathrm{w}_{,\mathrm{y}} \end{bmatrix}^{\mathrm{T}} \mathrm{h} \mathrm{d}\Omega + \frac{1}{2} \int_{\Omega} \mathrm{s}^2 \begin{bmatrix} \phi_{\mathrm{x,x}} & \phi_{\mathrm{x,y}} \end{bmatrix} \hat{\boldsymbol{\sigma}}^0 \begin{bmatrix} \phi_{\mathrm{x,x}} & \phi_{\mathrm{x,y}} \end{bmatrix}^{\mathrm{T}} \frac{\mathrm{t}^3}{12} \mathrm{d}\Omega + \\ + \frac{1}{2} \int_{\Omega} \mathrm{s}^2 \begin{bmatrix} \phi_{\mathrm{y,x}} & \phi_{\mathrm{y,y}} \end{bmatrix} \hat{\boldsymbol{\sigma}}^0 \begin{bmatrix} \phi_{\mathrm{y,x}} & \phi_{\mathrm{y,y}} \end{bmatrix}^{\mathrm{T}} \frac{\mathrm{t}^3}{12} \mathrm{d}\Omega \tag{12}$$

In this section, we study buckling of cracked plates. Firstly, the crack shape is defined by solving Eq. (10b) with function $\Psi(\mathbf{u})$ [20]

$$\Psi(\mathbf{u}) = B \frac{G_J}{4l} . H(x) \tag{13}$$

where

$$H(x) = \begin{cases} 1 & if \ x \le l_{crack} \ \ and \ \ \dfrac{-l_0}{2} \le y \le \dfrac{l_0}{2} \\ 0 & else \end{cases} \tag{14}$$

and the scalar B is taken in this work by $B = 10^3$.

The parameter s is computed by solving Eq. (10b), and take this value of s to Eq. (10a) to get buckling loads and buckling mode shapes.

Some main steps of the numerical solution procedure can be briefly summarized as follows:

(1) The first step is to discrete the structure domain and inputted data for problem.

(2) The second step is to model the crack shape by calculating function $\Psi(\mathbf{u})$ from Eq. (13).

(3) The next step is to determine the phase field s by solving Eq. (10b) and then calculate the element stiffness matrix $\boldsymbol{K}^{\mathrm{e}}$ and element tangent stiffness matrix $\boldsymbol{K}_{\mathrm{G}}^{\mathrm{e}}$ as Eqs. (11) and (12).

(4) The final step is to solve Eq. (10a) to find out the thermal critical buckling load λ_{cr} and mode shapes.

4. Numerical results and discussion

4.1. Neutral surface of FGM plate

In this paper, two kinds of FGM plate Al/ZrO_2 and Al/Al_2O_3 with material properties reported in Table 1 are considered. From Eq. (3) one can easily calculate the maximum value of h_0/h when the volume index fraction n_{max} is

$$n_{\max} = \sqrt{2 \frac{E_c}{E_m}} \tag{15}$$

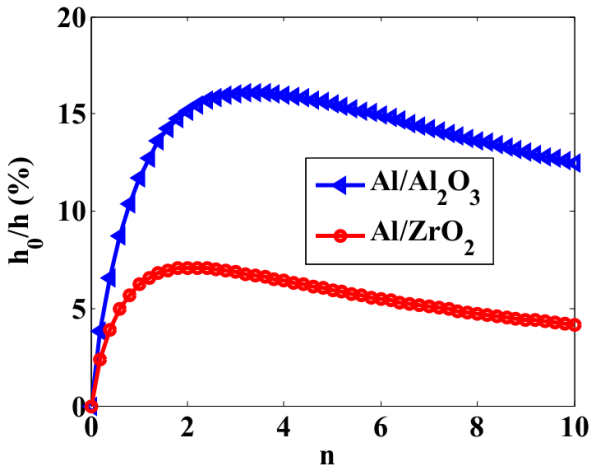

Fig. 2 Variation of h_0 as a function of n in two kinds of FGM

With FGM plate made of Al/ZrO_2 then $n_{max} \approx 2.07$ (h_0/h reaches the maximum value as 7.08%) and with Al/Al_2O_3 then $n_{max} \approx 3.3$ (h_0/h reaches the maximum value as 15.8%). The variation of n and its effect on value of h_0/h for two kinds of FGMs plates are shown in Figure 2. The thermal buckling of cracked FGM plates with or without considering the difference between neutral surface and mid-surface, which depends on h_0/h of each material, will be analyzed in subsequent sections.

4.2. Comparison of buckling of FGM plate and cracked FGM plate

The accuracy of the present formulation is first analyzed. To this end, we compare the thermal buckling of a fully clamped square FGM plate made of Al/Al_2O_3 (see Table 1 for its material properties). The plate geometry is given by $HxL = 0.2x0.2$ m^2 size, the thickness h (in two cases: H/h=50 and H/h=100). Table 2 reports the obtained results of the critical buckling temperature rise (CBTR) by the present method, which are compared with ones derived from the extended isogeometric analysis (XIGA) method [1] and the element-free *kp*-Ritz method [5]. From Table 2, it is obvious to see that the author results agree well with the reference solutions, reflecting the accuracy of the developed approach.

Table 1

Material parameters of functionally graded materials [1]

Material	Properties		
	E (GPa)	ν	α ($1/^0$C)
Aluminum (Al)	70	0.3	23.10^{-6}
Alumina (Al_2O_3)	380	0.3	$7.4.10^{-6}$
Zirconia (ZrO_2)	151	0.3	10.10^{-6}

Table 2

Comparison of the CBTR of a fully clamped square Al/Al_2O_3

H/h	Method	The volume fraction exponent (n)				
		0	0.5	1	2	5
100	XIGA [1]	45.265	26.650	21.033	18.646	19.231
	Ritz [5]	44.171	24.899	20.771	18.489	19.150
	This work	45.244	25.388	20.868	18.551	19.125
50	XIGA [1]	180.127	102.120	83.750	74.230	76.488
	Ritz [5]	175.817	99.162	82.357	71.013	74.591
	This work	179.809	100.955	83.001	73.780	75.994

Next we compare the thermal buckling of a fully simple supported square Al/ZrO_2 plate having a central crack as depicted in Figure 3. The plate geometry is given by H=L=1 m, plate thickness h = 0.01 m, crack length is c and c/H=0.6, $\theta = 0$. Comparison of the CBTR of this FGM plate is presented in Table 3 shows that the CBTR obtained by the present formulation is in good agreement with the reference solution through the XIGA method, also by the authors, [1].

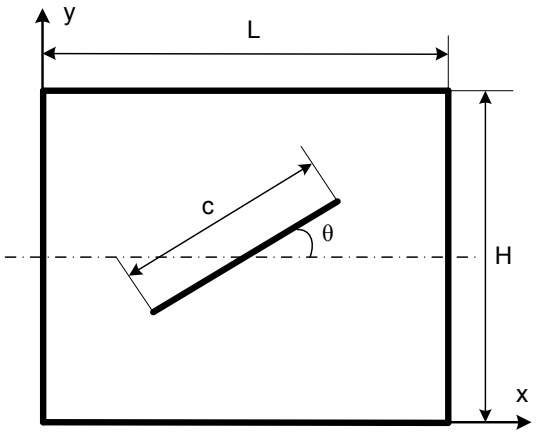

Fig. 3 The model geometry of a plate with an inclined central crack

Table 3

Comparison of the CBTR of a fully simple support square Al/ZrO_2 plate (c/H=0.6, H/L=1, $\theta = 0^0$)

Method	The volume fraction exponent (n)				
	0	0.5	1	2	5
XIGA [1]	8.894	6.114	5.412	5.012	4.771
This work	8.735	6.035	5.415	5.047	4.742

4.3. Analysis of thermal buckling of cracked FGM plates

4.3.1. Effect of volume index fraction n: L/H=1, L/h=50, $c/H = 0.2$, $\theta = 0$

The effect of material component fraction on thermal buckling is analyzed. It is accomplished by changing the volume fraction index n from 0 to 10. The geometry parameters of the FGM plate are as follows: L/H=1, thickness $h=H/50$, a central crack with its length c and c/H=0.2, crack angle $\theta = 0$ as depicted in Figure 4. We examine two cases, the first case is to analyse the difference between neutral surface and mid-surface; while the second case has no distance between two surfaces, i.e., they are identical. Three boundary conditions such as fully simple supported (SSSS), fully clamped (CCCC), two simple supported opposite edges and two clamped residual edges (CSCS) are considered. The FGM plate made of Al/Al_2O_3 and Al/ZrO_2 with material properties as Table 1. The CBTR results of these plates are shown in Figure 4. The percentage errors, which are calculated based on Eq.(16), between two cases for three boundary conditions are depicted in Figure 5.

$$\text{error}(\%) = \frac{CBTR(Mid) - CBTR(Neutral)}{CBTR(Neutral)} \times 100\% \tag{16}$$

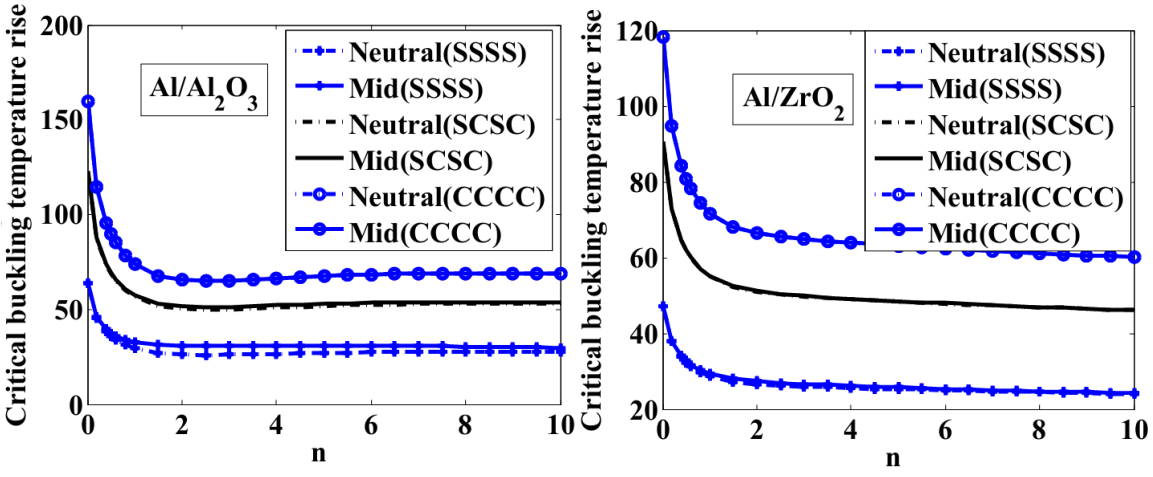

Fig. 4 Effect of volume fraction exponent and boundary condition on CBTR of cracked FGM plate

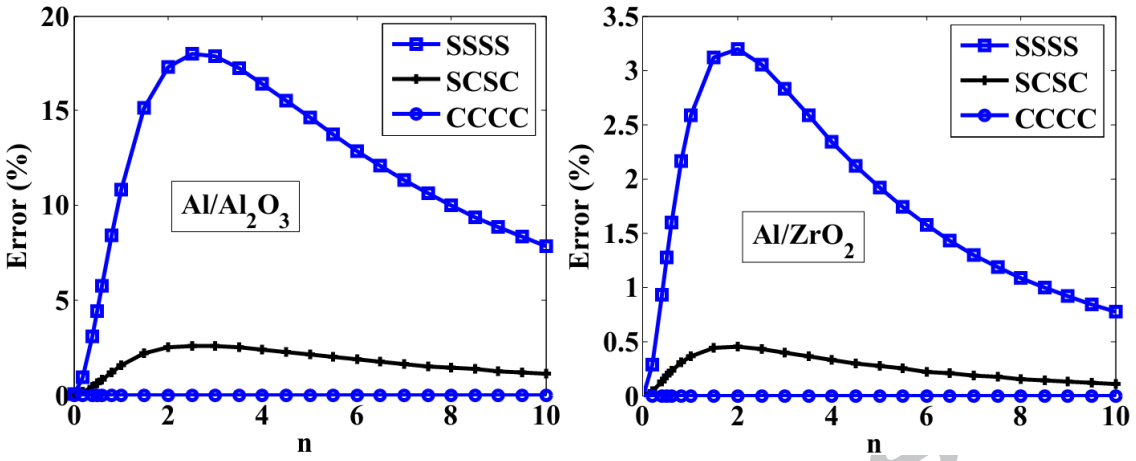

Fig. 5 Variation of boundary condition and its effect on CBTR' error between two cases (with and without distance between mid-surface and neutral-surface) as a function of n

When n increases, it is the same as the increase of metal fraction, the plate stiffness decreases, leading to the decrease of the thermal buckling critical of cracked plates. The error between two cases with SSSS plate is higher than that with CCCC and CSCS. However, from Figure 3, as $E_{Al2O3}/E_{Al} > E_{ZrO2}/E_{Al}$ that distance between neutral surface and mid-surface of Al/Al_2O_3 plate is higher than that of Al/ZrO_2 plate, so the error between two cases of Al/Al_2O_3 plate is higher than the error of Al/ZrO_2 plate. Specially for the Al/Al_2O_3 plate, when n >1, then the error is significant, i.e., >5%, the error even can reach upto 18%. This means that the difference between neutral surface and mid-surface with SSSS Al/Al_2O_3 plate must be taken into account and can not be neglected. In addition, it also indicates that the error between two cases depends on the Young modulus of ceramic and metal and also on the boundary condition.

4.3.2. Effect of crack length

The effect of crack length on the thermal buckling of cracked FGM plates is analyzed. We consider an FGM plate with L/H=1, thickness $h=H/50$, the volume fraction index n = 2, a crack angle $\theta = 0$, a crack length c changed with c/H=0.1-0.8, the obtained results of the CBTR are then shown in Figure 6. The error between two cases is also plotted in Figure 7.

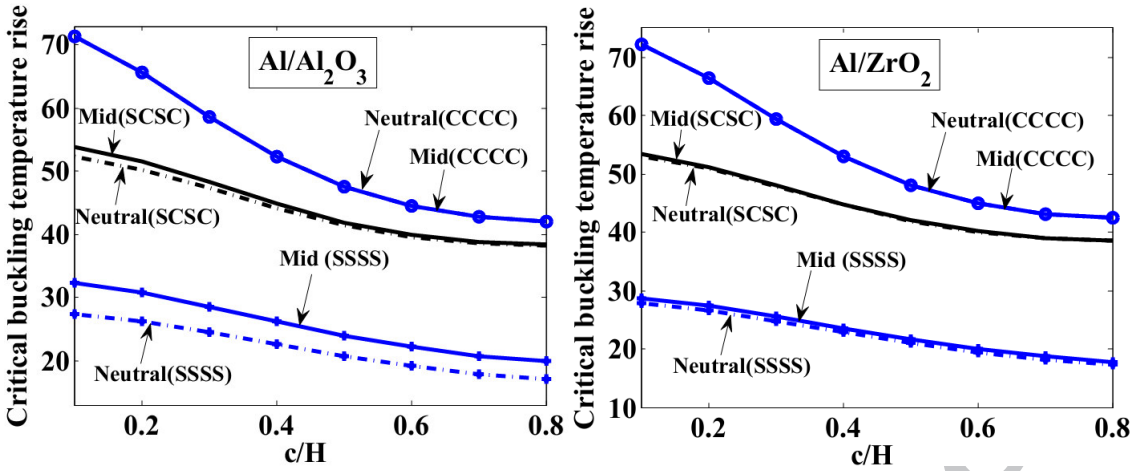

Fig. 6 Effect of crack length and boundary condition on CBTR of cracked FGM plate

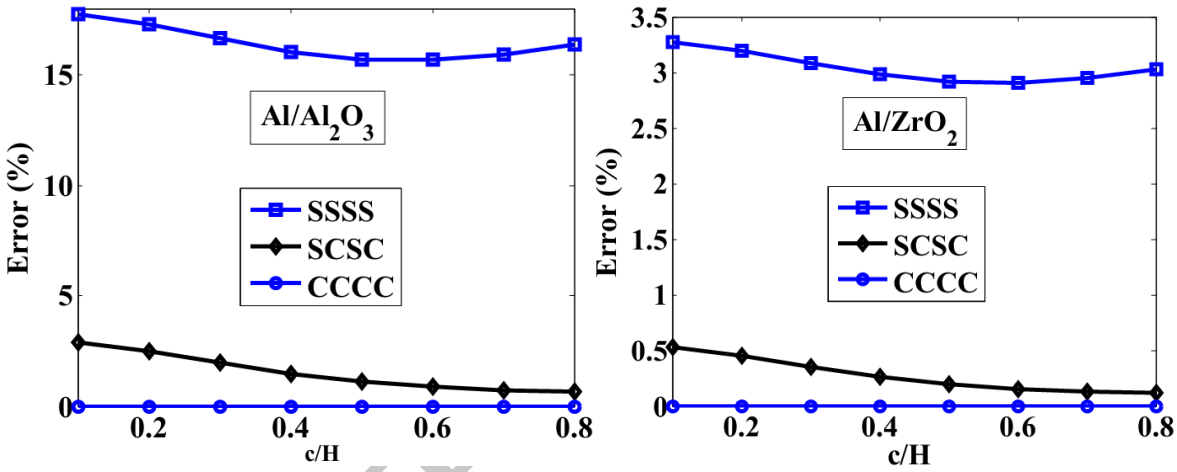

Fig. 7 Variation of boundary condition and its effect on CBTR' error between mid-surface and neutral-surface as a function of crack length

When *c/H* increases, or crack length increases, the plate stiffnes decrease, so that the thermal buckling critical of this plate decreases. The error between two cases with SSSS Al/Al_2O_3 plate > 15%, but it <3.5% with Al/ZrO_2 plate. The error is less than 4% for the plates with the two boundary conditions (CCCC and CSCS). As the above study, from Figure 5, we can also see that the error of Al/Al_2O_3 plate is larger than that of Al/ZrO_2. It may be due to the fact that the value of h_0 of Al/Al_2O_3 is larger than that of Al/ZrO_2.

The effect of the boundary conditions on the thermal buckling of cracked FGM plates is significant. Based on our own numerical experiments, we have found that the CCCC yields smaller error than other boundary conditions.

4.3.3. Effect of crack angle

The effect of crack angle on the thermal buckling of cracked FGM plates is studied. The FGM plate takes the same as the one presented in the previous subsection 4.2.3. The crack length *c/H*=0.2, crack angle increase from 15^0 to 60^0, the CBTR and the error between two case are presented in Tables 4 and 5, respectively. It can be seen that the crack angle of this plate has an insignificant effect on the critical thermal buckling. However, the boundary conditions again show a great impact on the solution. The CCCC plates yield largest values of the CBTR. The CNTR for SSSS plates with neural surface is smaller than that for the mid-surface, but it is similar for the CCCC plates.

Table 4

The CBTR of a square Al/Al_2O_3 plate (c/H=0.2, H/L=1, H/h=50, n=2)

BC	Reference plane	θ (^{0})							
		15		30		45		60	
		CBTR	Error (%)	CBTR	Error (%)	CBTR	Error (%)	CBTR	Error (%)
SSSS	Neutral	26.2101	17.27	26.2021	17.27	26.2036	17.26	26.2233	17.27
	Mid	30.7389		30.7273		30.7281		30.7534	
SCSC	Neutral	50.1634	2.51	49.7647	2.58	49.22	2.69	48.6931	2.82
	Mid	51.4266		51.0519		50.5463		50.0665	
CCCC	Neutral	65.6773	0	65.6401	0	65.6426	0	65.7259	0
	Mid	65.6773		65.6401		65.6426		65.7259	

Table 5

The CBTR of a square Al/ZrO_2 plate (c/H=0.2, H/L=1, H/h = 50, n=2)

BC	Reference plane	θ (^{0})							
		15		30		45		60	
		CBTR	Error (%)	CBTR	Error (%)	CBTR	Error (%)	CBTR	Error (%)
SSSS	Neutral	26.5484	3.19	26.5400	3.19	26.5411	3.19	26.5621	3.19
	Mid	27.3962		27.3872		27.3881		27.4102	
SCSC	Neutral	50.7875	0.45	50.3798	0.46	49.8232	0.48	49.2886	0.51
	Mid	51.0188		50.6155		50.0661		49.5402	
CCCC	Neutral	66.4555	0	66.4165	0	66.4172	0	66.5061	0
	Mid	66.4555		66.4165		66.4172		66.5061	

4.3.4. Effect of plate thickness*: L/H=1, c/H = 0.2,* $\theta = 0$ *, n =2*

The effect of plate thickness on the CBTR is considered. An FGM plate with *L/H*=1, *n* = 2, crack angle 0^0, *c/H* = 0.2, is considered. The plate thickness *h* varies from *L/h* = 20-100 is taken. The CBTR as a function of the plate thickness *h* is plotted in Figure 8 and the error between two cases is in Figure 9.

From these figures we can see that the plate thickness greatly affects the CBTR. The plate thickness increases with increasing the thermal buckling critical. The error is always higher than 16% with Al/Al_2O_3 and every thickness in fully simple supported boundary condition.

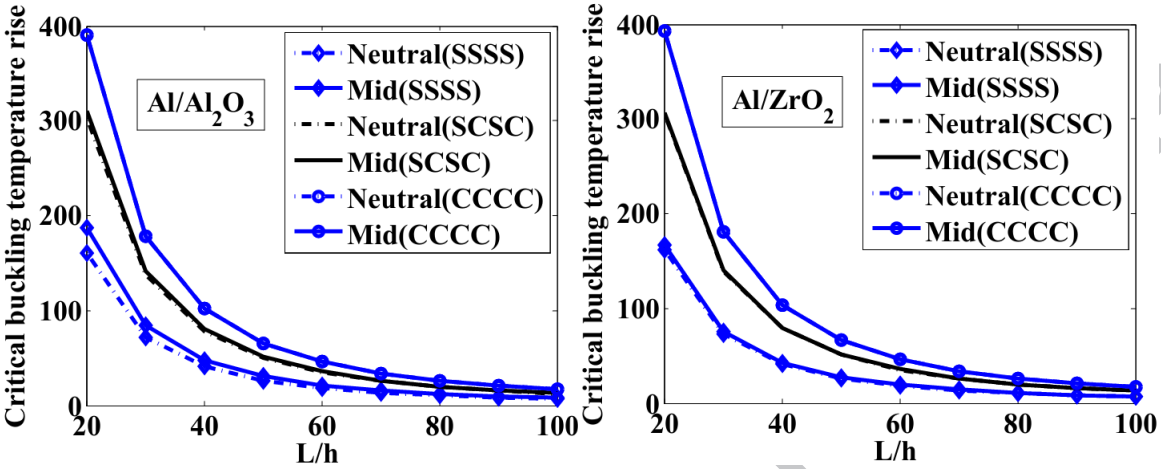

(b)

Fig. 8 Effect of aspect ratio L/h and boundary condition on CBTR of cracked FGM plate

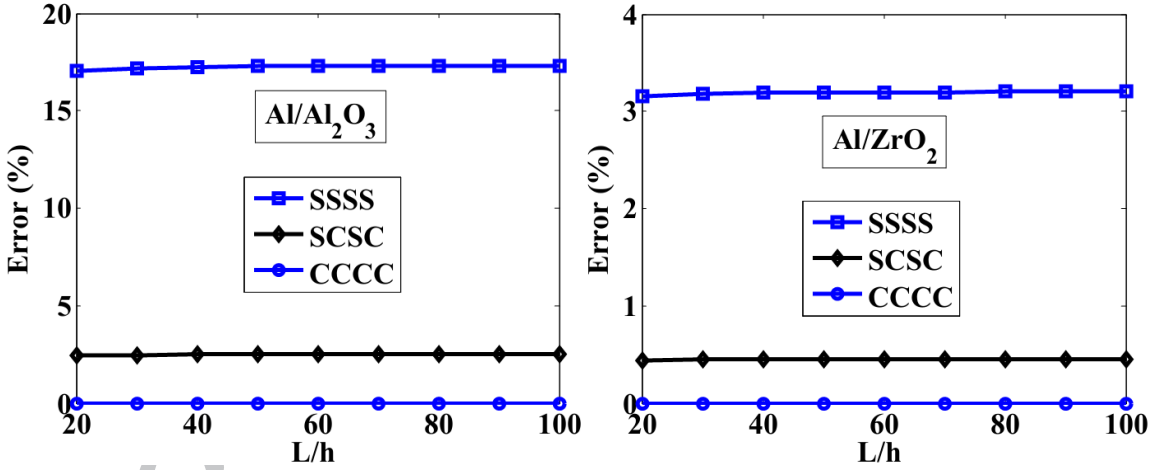

Fig. 9 Variation of boundary condition and its effect on CBTR' error between mid-surface and neutral-surface as a function of aspect ratio L/h

5. Conclusions

This work has outlined the development of an effective computational approach based on phase field model and Mindlin theory for studying thermal buckling of cracked FGM plates. We first derive the theory for the phase field model, which is particularly for thermal buckling analysis of cracked FGM plates, and then provide numerical examples. Two cases with and without difference between neutral surface and mid-surface are considered, and their obtained numerical results are analyzed in detail. The

present results are compared with the reference solutions based on XIGA and meshfree methods. Very good agreements are obtained. Through the above results, it indicates two major points: (a) The thermal buckling of cracked FGM plate is heavily dependent on the boundary condition, volume fraction index, plate thickness and crack length; (b) The error of the thermal buckling between two case (with and without difference between neutral surface and mid-surface) is also dependent on the Young modulus ratio E_c/E_m and the boundary condition. The results sudied in this paper show that with fully simple supported Al/Al_2O_3 plate, the error is always higher than 15%, so one cannot neglect the difference between neutral surface and mid-surface once studying the thermal buckling of cracked FGM plates. We believe that this information may be helpful in the design of FGM for engineering applications. Nevertheless, the limitation of the present work is just the first attempt of application of the phase field model to study thermal buckling of cracked FGM plates with inclined cracks. Further studies should be extended to study thermal buckling of FGM plates with arbitrary cracks, or multiple cracks.

Acknowledgments

NDD gratefully acknowledges the supports of Vietnam National University (VNU) under Project No. QG.17.45. TQB gratefully acknowledges the internal support of Tokyo Institute of Technology, Japan.

References

[1]. Tiantang Yu, Tinh Quoc Bui, Shuohui, Duc Hong Doan, C.T Wu, Thom Van Do, Satoyuki Tanaka (2016), "On the thermal buckling analysis of functionally graded plates with internal defects using extended isogeometric anlysis", *Composite Structures*, **136**, 684-695.

[2]. Tinh Quoc Bui , Thom Van Do, Lan Hoang That Ton, Duc Hong Doan, Satoyuki Tanaka, Dat Tien Pham, Thien-An Nguyen-Van, Tiantang Yu, Sohichi Hirose (2016), "On the high temperature mechanical behaviors analysis of heated functionally graded plates using FEM and a new third-order shear deformation plate theory" *Composite part B*, 92, 218-241.

[3]. Reddy J. N. (2000), "Analysis of Functionally Graded Plates" *Int. J. Number Meth. Engng*, **47**, 663-684.

[4]. Young-Hoon Lee, Seok-In Bae, Ji-Hwan Kim (2016), "Thermal buckling behavior of functionally graded plates based on neutral surface", *Comosite Structures*, **137**, 208-214.

[5]. Zhao X, Lee YY, Liew KM (2009), "Mechanical and thermal buckling analysis of functionally graded plates", *Composite Structures*, **90 (2)**, 161-171.

[6] Javaheri R, Eslami MR. Thermal buckling of functionally graded plates. AIAA J 2002;40(1):162–9.

[7] Shariat BAS, Eslami MR. Buckling of thick functionally graded plates under mechanical and thermal loads. Compos Struct 2007;78(3):433–9.

[8] Woo J, Meguid SA. Thermomechanical postbuckling analysis of functionally graded plates and shallow cylindrical shells. Acta Mech 2003;165(1–2):99–115.

[9] Najafizadeh MM, Heydari HR. Thermal buckling of functionally graded circular plates based on higher order shear deformation plate theory. Eur J Mech 2004;23(6):1085–100.

[10] Khalfi Y, Hourai MSA, Tounsi A. A refined and simple shear deformation theory for thermal buckling of solar functionally graded plates on elastic foundation. Int J Comput Methods 2014;11(5):1350071. 20P.

[11] Malekzadeh P. Three-dimensional thermal buckling analysis of functionally graded arbitrary straight-sided quadrilateral plates using differential quadrature method. Compos Struct 2011;93(4):1246–54.

[12] Shariat BA Samsam, Eslami MR. Thermal buckling of imperfect functionally graded plates. Int J Solids Struct 2006;43(14–15):4082–96.

[13] Jaberzadeh E, Azhari M, Boroomand B. Thermal buckling of functionally graded skew and trapezoidal plates with different boundary conditions using the element-free Galerkin method. Eur J Mech 2013;42:18–26.

[14] Zhao X, Lee YY, Liew KM. Mechanical and thermal buckling analysis of functionally graded plates. Compos Struct 2009;90(2):161–71.

[15] Zhang DG. Modeling and analysis of FGM rectangular plates based on physical neutral surface and high order shear deformation theory. Int J Mech Sci 2013;68:92–104.

[16] Zhang DG, Zhou YH. A theoretical analysis of FGM thin plates based on physical neutral surface. Comput Mater Sci 2008;44:716-20.

[17] Yaghoobi H, Fereidoon A. Influence of neutral position on deflection of functionally graded beam under uniformly distributed. World AppISci J 2010;10:337-41.

[18] Miehe C, Hofacker M, Welschinger F. A phase field model for rate-independent crack propagation: robust algorithmic implementation based on operator splits. Comput Meth Appl. Mech Eng 2010; 199:2766-2778.

[19] Doan HD, Bui QT, Nguyen DD, Fushinobu K. Hybrid phase field simulation of dynamic crack propagation in functionally graded glass-filled epoxy. Compos Part B: Engin 2016; 99:266-276.

[20] Michael JB, Clemens VV, Michael AS, Thomas JRH, Chad ML. A phase-field description of dynamic brittle fracture. Comput. Methods Appl. Mech. Engrg. 2012; 217–220: 77–95.

[21] Yao WA, Hu XF. A novel singular finite element of mixed-mode crack problems with arbitrary crack tractions. Mech Rese Commu 2011; 38(3): 170-175.

[22] Hu XF, Chen BY, Trivaudey M, Tan VBC, Tay TE. Integrated XFEM-CE analysis of delamination migration in multi-directional composite laminates. Composites Part A: Appl Scie Manufac 2016; 90: 161-173.

[23] Hu XF, Bui TQ, Wang J, Yao W, Ton LHT, Singh IV, Tanaka S. A new cohesive crack tip symplectic analytical singular element involving plastic zone length for fatigue crack growth prediction under variable amplitude cyclic loading. European Journal of Mechanics-A/Solids 2017; 65: 79-90.

[24] Hu XF, Yao WA. A new enriched finite element for fatigue crack growth. International Journal of Fatigue 2013; 48: 247-256.